Cellular Physiology and Biochemistry

Cell Physiol Biochem 2026;60:646-658
DOI: 10.33594/000000900
Published online: 18 November 2026
Accepted: 1 October 2026

© 2026 The Author(s)
Published by Cell Physiol Biochem Press GmbH&Co. KG, Duesseldorf
www.cellphysiolbiochem.com

This article is licensed under the Creative Commons Attribution 4.0 International License (CC BY). This means that any user shall be free to copy and redistribute the material in any medium or format, also for commercial purposes, provided proper credit is given to the Authors as well as the original publisher.

Original Paper

Andrographolide Induces Apoptosis in Burkitt's Lymphoma by Suppressing Antioxidant Defense Rather Than Ferroptosis

Haiyun Liu[a] Bo Ke[b] Tiantian Wang[c] Tingting Liu[b] Quangang Fang[a]

[a]Department of Clinical Laboratory, Jiangxi Provincial People's Hospital, The First Affiliated Hospital of Nanchang Medical College, Nanchang, Jiangxi, China, [b]Department of Hematology, Jiangxi Provincial People's Hospital, The First Affiliated Hospital of Nanchang Medical College, Nanchang, Jiangxi, China, [c]Jiangxi University of Chinese Medicine, Nanchang, Jiangxi, China

Key Words
Andrographolide • Burkitt's lymphoma • Apoptosis • Ferroptosis

Abstract
Background/Aims: This study aimed to investigate whether andrographolide (AD) exerts cytotoxic effects on Burkitt's lymphoma cells by inducing ferroptosis. ***Methods:*** Burkitt's lymphoma cell lines CA46 and Raji were cultured *in vitro*. AD-induced cytotoxicity was assessed using the CCK-8 assay and AO/PI staining. Ferroptosis involvement was evaluated through ferroptosis inhibitor rescue assays and ferroptosis-related biochemical analyses. Western blotting was performed to measure the expression of apoptosis-related proteins (cleaved caspase-3, Bcl-2, Bax), ferroptosis-related proteins (GPX4, xCT, ACSL4), and the phosphorylation levels of Nrf2. Additionally, reactive oxygen species (ROS) generation following AD treatment was analyzed by DCFH-DA staining. Mitochondrial membrane potential was measured using JC-1 fluorescence staining. ***Results:*** AD treatment significantly reduced the viability of CA46 and Raji cells, and this cytotoxicity was not rescued by the ferroptosis inhibitor Ferrostatin-1. AO/PI staining revealed a marked increase in PI-positive cells upon AD treatment. Biochemical assays showed no significant changes in malondialdehyde (MDA) levels or ferrous iron (Fe^{2+}) content after AD exposure. Western blot analyses indicated no significant alteration in xCT expression, while ACSL4 protein levels were downregulated and GPX4 levels were upregulated following AD treatment. Moreover, Nrf2 phosphorylation was significantly decreased, concurrent with increased expression of apoptosis markers cleaved caspase-3 and Bax and decreased Bcl-2 expression. Mitochondrial membrane depolarization was observed in AD-treated cells. DCFH-DA fluorescence imaging demonstrated a substantial increase in intracellular ROS in AD-treated cells. The ROS scavenger NAC markedly attenuated AD-induced cell death as shown by AO/PI staining and reduced the upregulation of cleaved

Quangang Fang
Department of Clinical Laboratory, Jiangxi Provincial People's Hospital, The First Affiliated Hospital of Nanchang Medical College, 152 Aiguo Road, Nanchang 330006, Jiangxi, China.
E-Mail: fqg173224668@163.com

caspase-3 ($P < 0.05$); NAC also partially restored Nrf2 phosphorylation ($P < 0.05$). ***Conclusion:*** AD inhibits Burkitt's lymphoma cell viability primarily by inducing apoptosis rather than ferroptosis.
© 2026 The Author(s). Published by Cell Physiol Biochem Press GmbH&Co. KG

Introduction

Burkitt's lymphoma is a rare and highly aggressive subtype of B-cell lymphoma that predominantly affects children and young adults. It accounts for 1 to 2% of non-Hodgkin's lymphomas in adults [1]. The rapid growth and spread of lymphoma cells to extranodal anatomical sites such as the intra-abdominal organs and central nervous system are significant clinical features in patients with Burkitt's lymphoma [2]. Moreover, the onset of this lymphoma has been associated with the Epstein-Barr virus (EBV) and translocation of the MYC oncogene. Genomic studies have shown the presence of mutations in p53 and along the phosphatidylinositol 3-kinase (PI3K) signaling pathway that contribute to oncogenesis [3, 4].

The cornerstone of Burkitt's lymphoma treatment remains chemotherapy, which has demonstrated remarkable efficacy in managing the disease and improving patient outcomes. Combination chemotherapy can significantly improve the cure rate of Burkitt's lymphoma. In selected cases, new immunotherapeutic approaches such as chimeric antigen receptor T-cell (CAR-T) therapy or stem cell transplantation may also be considered as therapeutic modalities to further augment treatment efficacy [5]. However, the prognosis of Burkitt's lymphoma varies widely, depending on the specific disease type and stage at diagnosis, highlighting the importance of early detection and prompt initiation of treatment to optimize patient outcomes. Patients with chemotherapy-refractory disease have few effective salvage options and a median overall survival of less than 3 months [6], underscoring a clear clinical need for agents with novel mechanisms of action.

Ferroptosis is a form of regulated cell death characterized by iron-dependent accumulation of reactive oxygen species (ROS) and subsequent peroxidation of membrane lipids, ultimately leading to cellular damage and death. The onset of ferroptosis is governed by the balance between opposing suppressive and promoting arms, with the suppressive arm centered on the system Xc^--GSH-GPX4 axis [7]. Upstream of this axis, Nrf2 serves as the master regulator of the cellular antioxidant response. Mechanistically, upon oxidative stimulation, Nrf2 dissociates from Keap1, translocates into the nucleus and initiates transcription of target genes, including SLC7A11, GPX4 and the GSH-synthesizing enzyme system [8]. Notably, SLC7A11 enhances cystine uptake to fuel GSH synthesis, which in turn provides reducing equivalents for GPX4 to detoxify lipid peroxides, thereby reinforcing the system Xc^--GSH-GPX4 axis and constituting a key defense against ferroptosis. Given this regulatory framework, emerging evidence indicates that Burkitt's lymphoma exhibits marked vulnerability to ferroptosis. Pharmacological induction of ferroptosis in Burkitt's lymphoma cells confers significant antitumor activity, and therapeutic modulation of ferroptotic pathways can potentiate treatment efficacy against this aggressive lymphoma subtype [9, 10]. Consequently, targeting ferroptosis-related molecular mediators represents a promising therapeutic strategy to control disease progression and circumvent resistance to conventional chemotherapeutic regimens [11].

Andrographolide (AD), a naturally occurring compound derived from a traditional herbal medicine *Andrographis paniculata*, belongs to the diterpenoid lactone class of compounds and has garnered significant attention for its diverse medicinal properties [12]. AD has been reported to exhibit a wide range of biological effects including anti-inflammatory, antibacterial, antioxidative, antiviral, antiplatelet, antidiarrheal, hypoglycemic, hypolipidemic, hepatoprotective, neuroprotective, and hypotensive activities, as well as therapeutic benefits in Parkinson's disease and musculoskeletal disorders [13-17]. In addition, accumulating evidence has demonstrated that AD possesses antitumor activity in multiple cancer cell types. Specifically, AD has been shown to suppress tumor

progression through the induction of ferroptosis in lung cancer [18], pancreatic cancer [19], multiple myeloma [20] and T-cell acute lymphoblastic leukemia (T-ALL) [21]. Despite these promising findings, it remains unclear whether AD induces ferroptosis in Burkitt's lymphoma. Of particular relevance to Burkitt's lymphoma, previous studies have shown that AD can inhibit the proliferation of multiple tumor cell lines and induce apoptosis, suggesting its potential use as an anti-Burkitt's lymphoma agent [22, 23].

In this study, we aimed to investigate whether AD exerts cytotoxic effects on Burkitt's lymphoma cells through ferroptosis or alternative mechanisms and to elucidate the underlying pathways, thereby establishing a basis for therapeutic interventions in Burkitt's lymphoma and other malignancies.

Materials and Methods

Cells and reagents

The Burkitt's lymphoma cell lines (CA46 and Raji), fetal bovine serum and RPMI 1640 medium were purchased from Procell (Wuhan, China). Andrographolide and Ferrostatin-1 were obtained from MCE (Shanghai, China). N-acetyl-L-cysteine (NAC) was purchased from Beyotime (Shanghai, China). JC-1 mitochondrial membrane potential fluorescent probe was purchased from Solarbio (Beijing, China). Cell culture plates and flasks were acquired from Servicebio (Wuhan, China). CCK-8 kit, ECL ultrasensitive luminescent solution and PAGE gel preparation kit were purchased from Solarbio (Beijing, China). The cell malondialdehyde (MDA) colorimetric assay kit and cell ferrous iron colorimetric assay kit were purchased from Elabscience (Wuhan, China). Rabbit anti-human B-cell lymphoma 2-associated X protein (Bax), B-cell lymphoma 2 (Bcl-2), and amino acid transport system Xc-(xCT/SLC7A11) primary antibodies were purchased from Abcam (Cambridge, UK). Rabbit anti-human NF-E2-related factor 2 (Nrf2), Phospho-Nrf2 (Ser40), glutathione peroxidase 4 (GPX4), and long-chain-fatty-acid-CoA ligase 4 (ACSL4) primary antibodies were purchased from HUABIO (Hangzhou, China). Rabbit anti-human cleaved caspase-3, caspase-3 and horseradish peroxidase (HRP)-conjugated secondary antibodies were purchased from Beyotime (Shanghai, China). Mouse anti-human glyceraldehyde-3-phosphate dehydrogenase (GAPDH) primary antibodies were purchased from Proteintech (Wuhan, China). FITC-conjugated secondary antibody was purchased from Yeasen (Shanghai, China). AO/PI fluorescence staining kits and DCFH-DA probe were purchased from Beyotime (Shanghai, China) and UElandy (Suzhou, China), respectively. A microplate reader was purchased from Thermo Fisher (Waltham, USA), a cell counter was provided by Countstar (Shanghai, China), and an inverted fluorescence microscope was provided by Leica (Wetzlar, Germany). Vertical electrophoresis, membrane transfer and chemiluminescent imaging systems were purchased from BioRad (Hercules, USA).

Cell culture and grouping

The cells were maintained in RPMI 1640 medium supplemented with 10% fetal bovine serum (FBS), at 37°C in a humidified incubator with 5% carbon dioxide. The culture medium was replaced every 48 hours to ensure optimal growth conditions for the cells. For experimental purposes, cells were suspended in fresh medium after centrifugation, followed by seeding in 96-well or 6-well plates for further experiments. Different concentrations of AD (0-500 μM) were added to the treatment groups. The Ferrostatin-1 solution (final concentration 2 μM, prepared in DMSO) was added to the AD + Ferrostatin-1 group.

Cell viability assay

CA46 and Raji cells were seeded in 96-well plates at a density of 1×10^4 cells/well (100 μL per well) and treated with varying concentrations of AD (10, 50, 100, or 500 μM) or vehicle control, in the presence or absence of Ferrostatin-1 (2 μM). After 24 hours of treatment, 10 μL of CCK-8 reagent was added to each well, followed by an additional 2-hour incubation. Optical density (OD) was measured at 450 nm using a microplate reader. Cell viability was expressed as a percentage of the vehicle-treated control group (defined as 100% viability) and represents the mean ± standard deviation of three independent experiments.

Acridine orange (AO)/propidium iodide (PI) fluorescence staining

CA46 and Raji cells were seeded in 12-well plates at a density of 1×10^5 cells/well (in 1 mL of complete medium per well) and treated with varying concentrations of AD or vehicle control. After 24 hours of treatment, cell suspensions were harvested. Equal volumes of the cell suspension and the AO/PI staining solution were gently mixed. Subsequently, 20 μL of the cell-stain mixture was loaded into a cell counting chamber. Cell fluorescence was then quantified using a cell counter equipped with fluorescence detection capabilities.

Malondialdehyde (MDA) colorimetric assay

CA46 and Raji cells were seeded in 6-well plates at a density of 1×10^6 cells per well (2 mL complete medium per well) and treated with AD at different concentrations, or with the vehicle control. After 24 h of incubation, cells were harvested, washed with cold PBS, and lysed according to the protocol of the Enhanced Cell Malondialdehyde (MDA) Colorimetric Assay Kit. An appropriate volume of working reagent was added to each cell lysate, and the mixture was incubated at 100 °C for 40 min. Samples were then allowed to cool to room temperature under a stream of running water, followed by centrifugation at 1100 × g for 10 min. The supernatants were transferred to a fresh 96-well plate and the absorbance was measured at 532 nm using a microplate reader. MDA concentrations were calculated by interpolation from a standard curve generated with the kit's MDA standards.

Ferrous iron (Fe^{2+}) colorimetric assay

CA46 and Raji cells were seeded in 12-well plates at a density of 1×10^6 cells per well (1 mL complete medium per well) and treated with AD at different concentrations, or with the corresponding vehicle control. After 24 h of incubation, cells were harvested and lysed on ice for 10min. The lysates were then cleared by centrifugation at 15000 × g for 10 min. According to the protocol of Cell Ferrous Iron Colorimetric Assay Kit , the supernatants were transferred to a fresh 96-well plate and mixed with the appropriate volume of working reagents. The reaction mixture was incubated at 37°C for 10 min, and the absorbance was measured at 593 nm using a microplate reader. The concentration of ferrous iron (Fe^{2+}) in each sample was then calculated using the equation provided in the kit manual.

Western blot analysis

CA46 and Raji cells were cultured in 6-well plates at a density of 1×10^6 cells/well (in 2 mL of complete medium per well) and treated with varying concentrations of AD or vehicle control. Following 24 hours of treatment, cell suspensions were harvested. Cell pellets were lysed on ice for 30 minutes using RIPA lysis buffer supplemented with protease and phosphatase inhibitors. After centrifugation at 12000 rpm for 2 min at 4°C, the supernatant was collected. Total protein concentration was quantified using the BCA protein assay. Equal amounts of total protein (20 μg per sample) were separated by SDS-PAGE and then transferred to a PVDF membrane using a semi-dry transfer system. The membrane was blocked with 10% non-fat dry milk in PBST at room temperature for 2 hours. Subsequently, the membrane was incubated with primary antibodies specific for each target protein overnight at 4°C. After extensive washing with PBST, the membrane was incubated with the appropriate HRP-conjugated secondary antibodies at room temperature for 2 hours. Following further washing with PBST, protein bands were detected using enhanced chemiluminescence (ECL) reagents and visualized with a chemiluminescent imaging system. Densitometric analysis of the protein bands was performed using ImageJ software, and the relative expression levels of target proteins were normalized to GAPDH.For phosphorylated Nrf2, the band intensity of the phosphorylated form was normalized to that of total Nrf2.

Intracellular ROS assay

CA46 and Raji cells were cultured in 12-well plates at a density of 1×10^5 cells/well (in 1 mL of complete medium per well) and treated with varying concentrations of AD or vehicle control. After 24 hours of treatment, cells were harvested and washed. The harvested cells were then resuspended in serum-free medium containing DCFH-DA at a final concentration of 10 μM. The cell suspensions were incubated for 30 minutes at 37°C in the dark to allow for intracellular ester hydrolysis and ROS oxidation. Following incubation, cells were washed once with serum-free medium to remove extracellular probe. Finally, the stained cells were mounted on glass slides and observed, and representative images were captured using a fluorescence microscope.

JC-1 Fluorescence Staining

CA46 and Raji cells were seeded in 12-well plates and treated with various concentrations of AD for 24 hours. Cells were then washed with PBS and incubated with JC-1 working solution at 37° C in the dark for 20 min. Following incubation, cells were washed with RPMI 1640 medium and immediately examined under a fluorescence microscope. Mean fluorescence intensity (MFI) was quantified using ImageJ software. Mitochondrial membrane potential (MMP) was determined from the JC-1 monomer/aggregate fluorescence ratio.

Immunofluorescence assay

CA46 and Raji cells were seeded in 12-well plates and treated with various concentrations of AD for 24 h. After fixation with 4% paraformaldehyde for 15 min at room temperature, cells were permeabilized with 0.5% Triton X-100 and blocked with 5% BSA for 30 min. Cells were then incubated with anti-Nrf2 antibody (1:200) at 4°C overnight, followed by FITC-conjugated secondary antibody (1:300) for 1 h in the dark. Nuclei were counterstained with DAPI for 5 min, and images were captured using a fluorescence microscope.

Statistical Analysis

For statistical analysis, all data were expressed as means ± SD. Statistics were compared using GraphPad Prism version 9 (GraphPad Software, San Diego, CA, USA). The statistical differences were analyzed using a one-way analysis of variance (ANOVA) followed by Tukey's honestly significant difference (HSD) post hoc test. Statistical significance was denoted on charts with "*", "**", "***","****" or "ns" indicating p-value as $P < 0.05$, $P < 0.01$, $P < 0.001$, $P < 0.0001$or $P > 0.05$, respectively.

Results

AD inhibited the viability of Burkitt's lymphoma cells

The results of the CCK-8 assay showed that CA46 and Raji cells treated with AD had significantly lower cellular viability compared to the control group. Furthermore, the results of AO/PI staining showed that the number of PI-positive cells was significantly increased in treatment groups, indicating that AD decreased the viability of Burkitt's lymphoma cells (Fig. 1A-C).

AD failed to induce ferroptosis in Burkitt's lymphoma cells

CA46 and Raji cells were treated with AD for 24 h, either alone or in combination with the ferroptosis inhibitor Ferrostatin-1 (2 μM). CCK-8 assays revealed comparable cell viability between the AD-treated group and the AD + Ferrostatin-1 group (Fig. 2A), suggesting that ferroptosis was not the primary mode of cell death. Biochemical analysis further demonstrated that AD treatment did not significantly alter the levels of malondialdehyde (MDA) or ferrous iron (Fe^{2+}) (Fig. 2B, 2C), key markers of ferroptosis. Consistent with these findings, Western blot analysis showed no significant changes in the expression of xCT compared to untreated controls. Notably, the protein levels of ACSL4, a pro-ferroptotic enzyme, were downregulated following AD treatment, whereas GPX4 expression was increased (Fig. 3A), further confirming that AD does not trigger ferroptosis in Burkitt's lymphoma cells. Additionally, we examined the expression and phosphorylation of Nrf2, a critical antioxidant transcription factor. Intriguingly, phosphorylated Nrf2 was significantly downregulated in AD-treated cells (Fig. 3B), suggesting that AD may induce oxidative stress independent of ferroptosis. Taken together, these results indicate that while AD does not promote ferroptosis, it may exert its cytotoxic effects through oxidative stress mechanisms in Burkitt's lymphoma cells.

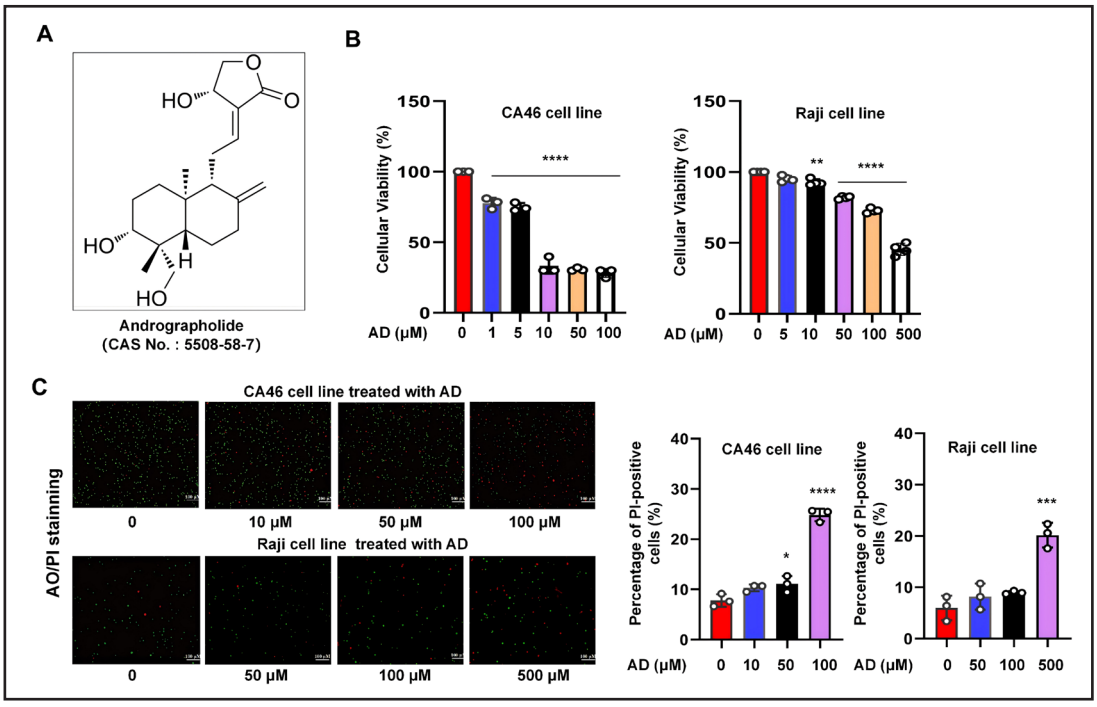
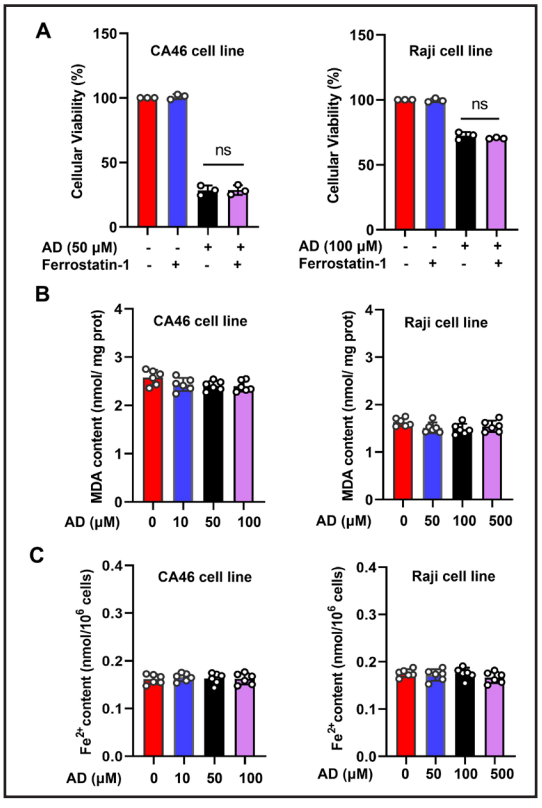


Fig. 1. AD inhibited the viability of Burkitt's lymphoma cells. (A) The chemical structure of AD. (B) The cell viability of Burkitt's lymphoma cells was determined by CCK-8 assay. The data shown represent percentage viability compared to control. (C) AO/PI fluorescence staining was performed to determine the apoptosis. *P<0.05 vs. control group, **P<0.01 vs. control group, ***P<0.001 vs. control group, ****P<0.0001 vs. control group. Experiments were performed in triplicate (n = 3).

Fig. 2. AD failed to induce ferroptosis in Burkitt's lymphoma cells. (A) Ferroptosis involvement was evaluated through ferroptosis inhibitor rescue assays. Experiments were performed in triplicate (n = 3). (B, C) The contents of MDA and Fe2+ in Burkitt's lymphoma cells were determined by colorimetry (n = 6). "ns" indicating P > 0.05 between "AD" group and "AD + Ferrostatin-1" group.



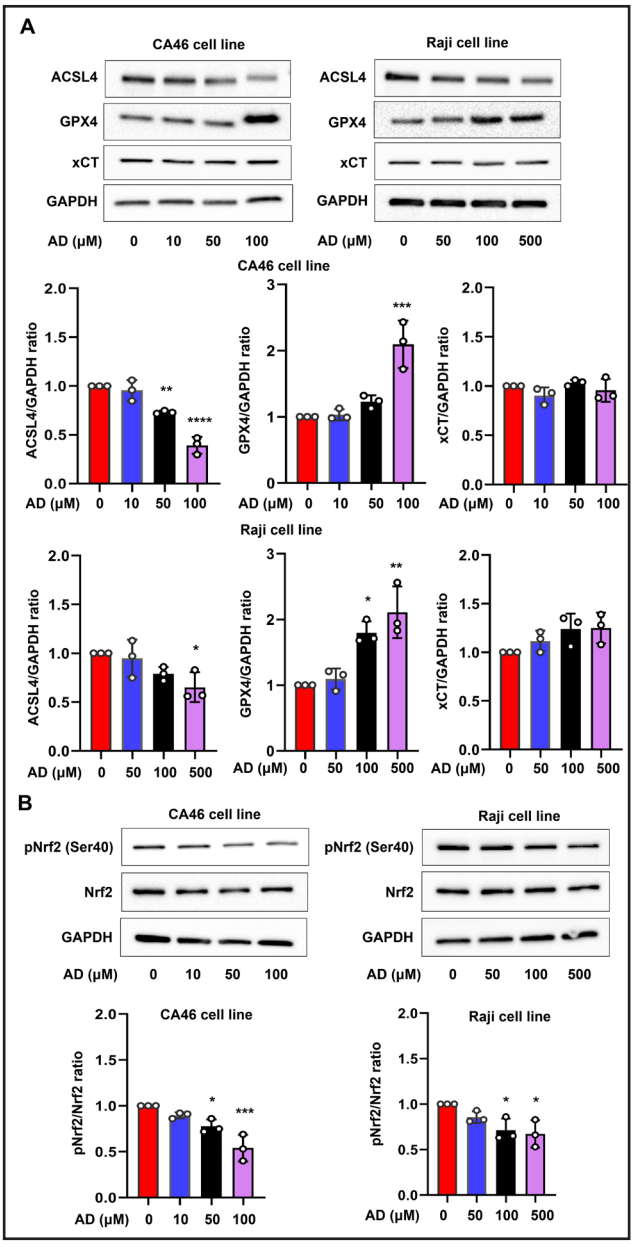


Fig. 3. The effects of AD on the expression of ferroptosis-related proteins and the phosphorylation level of Nrf2. (A) Representative Western blots and quantitative analysis of the ferroptosis associated proteins GPX4, xCT and ACSL4 in Burkitt's lymphoma cells. (B) Representative Western blots and quantitative analysis of the phosphorylation level of Nrf2 in Burkitt's lymphoma cells. *P<0.05 vs. control group, **P<0.01 vs. control group, ***P<0.001 vs. control group, ****P<0.0001 vs. control group. Experiments were performed in triplicate (n = 3).

AD induced the production of ROS and triggered apoptosis in Burkitt's lymphoma cells

The results above indicated that AD treatment diminished the phosphorylation status and functional activity of Nrf2, implying a compromise of the intracellular antioxidant defense system. To assess the consequent oxidative stress, intracellular ROS levels were measured. DCFH-DA fluorescence imaging revealed a pronounced increase in green fluorescence in AD-treated Burkitt's lymphoma cells, reflecting markedly elevated ROS production (Fig. 4A). Moreover, Western blotting analysis showed that AD exposure upregulated the expression of cleaved caspase-3 (P<0.05), a key executioner of apoptosis, concomitant with a marked decrease in pro-caspase-3 levels (Fig. 4B). These findings confirm that AD induces apoptotic cell death in these lymphoma cells.

AD modulates the expression of Bcl-2 family proteins in Burkitt's lymphoma cells

Based on the observed increase in ROS and the onset of apoptosis, we hypothesized that AD induces cell death via the intrinsic (mitochondrial) apoptotic pathway. To test this

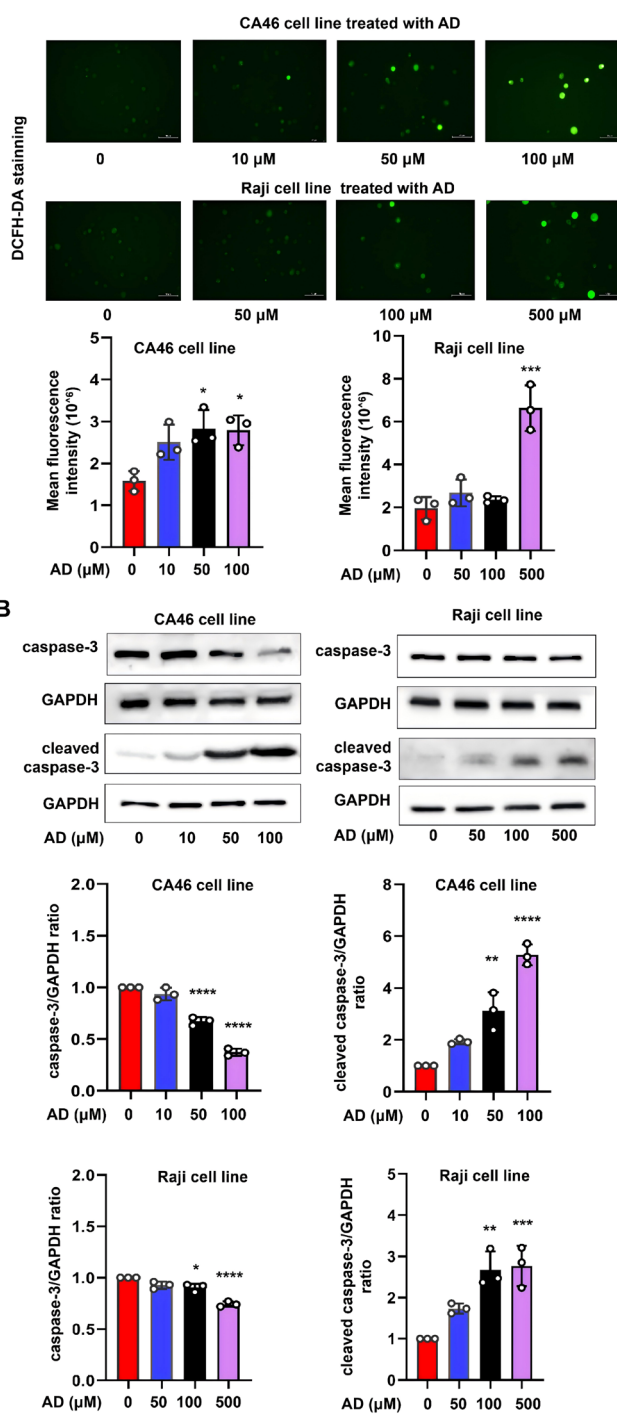


Fig. 4. AD induced the production of ROS and triggered apoptosis in Burkitt's lymphoma cells. (A) DCFH-DA staining was performed to detect the production of ROS. (B) Representative Western blots and quantitative analysis of caspase-3 and cleaved caspase-3. *P<0.05 vs. control group, **P<0.01 vs. control group, ***P<0.001 vs. control group, ****P<0.0001 vs. control group. Experiments were performed in triplicate (n = 3).

hypothesis, we evaluated the expression of the Bcl-2 family proteins Bax (pro-apoptotic) and Bcl-2 (anti-apoptotic). Compared to the control group, the expression of Bax was significantly increased in the AD-treated group ($P < 0.05$), whereas the expression of Bcl-2 was decreased ($P < 0.05$) (Fig. 5A). JC-1 fluorescence staining revealed that AD treatment significantly increased monomeric JC-1 (green fluorescence) while markedly decreasing aggregated JC-1 (red fluorescence) in Burkitt's lymphoma cells, resulting in a significantly elevated green/red fluorescence ratio ($P<0.05$) (Fig. 5B). These findings indicate mitochondrial membrane depolarization, confirming that AD induces cytotoxicity through the intrinsic apoptotic pathway.

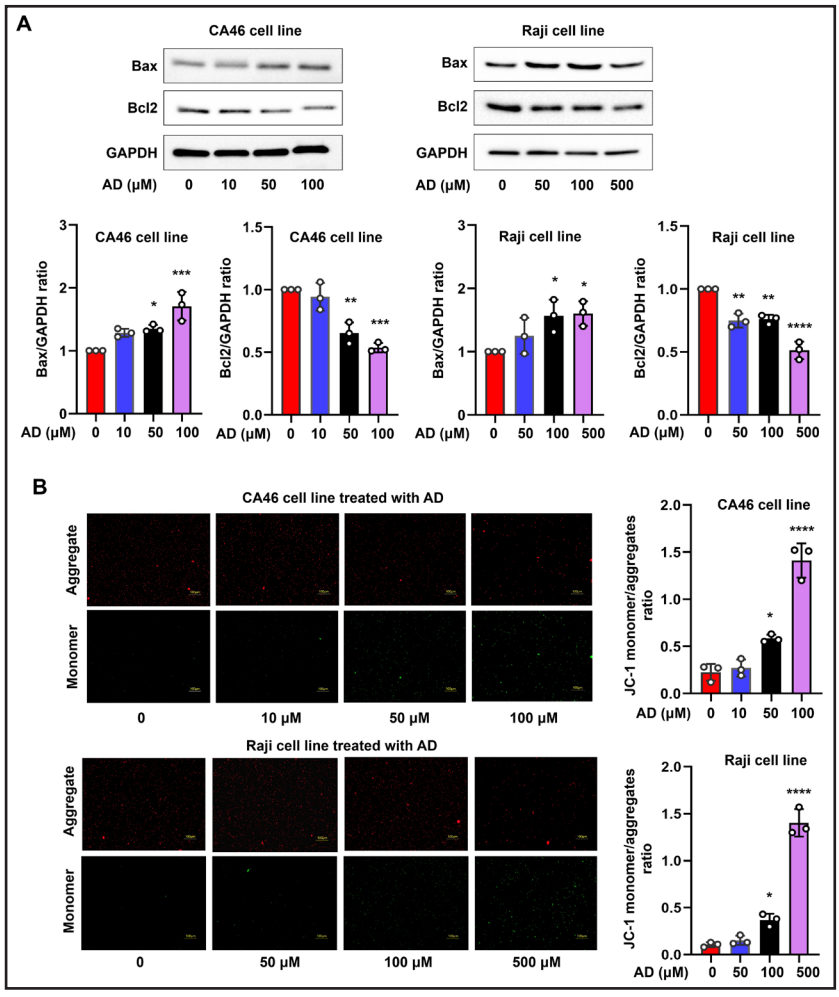


Fig. 5. AD modulates the expression of Bax and Bcl-2 in Burkitt's lymphoma cells. (A) Representative Western blots and quantitative analysis of the pro-apoptotic protein Bax and the anti-apoptotic protein Bcl-2 after treatment with AD. (B) Mitochondrial membrane potential (MMP) was assessed by JC-1 fluorescence staining. Representative images and quantitative analysis of MMP based on the JC-1 monomer/aggregate ratio are shown. *P<0.05 vs. control group, **P<0.01 vs. control group, ***P<0.001 vs. control group, ****P<0.0001 vs. control group. Experiments were performed in triplicate (n = 3).

NAC alleviated AD-induced cytotoxic effects on Burkitt's lymphoma cells

Elevated intracellular ROS act as second messengers that can trigger the intrinsic apoptotic pathway when their production overwhelms the capacity of cellular antioxidant defenses. Our data demonstrate that AD markedly increases ROS generation and concomitantly reduces Nrf2 phosphorylation in Burkitt's lymphoma cells, suggesting a link between ROS accumulation and apoptosis. To test whether ROS are causally responsible for the observed cytotoxicity, we pre-treated the cells with NAC, a well-characterized ROS scavenger. AO/PI staining revealed that NAC significantly mitigated AD-induced cell death ($P < 0.05$) (Fig. 6A). Consistently, Western blot analysis showed that NAC partially restored Nrf2 phosphorylation and attenuated the AD-mediated up-regulation of cleaved caspase-3 ($P < 0.05$) (Fig. 6B). AD-treated cells exhibited characteristic karyorrhexis, concomitant with a marked decrease in nuclear Nrf2 levels. Notably, NAC intervention significantly attenuated karyorrhexis and restored the nuclear localization of Nrf2 (Fig. 6C), suggesting that AD-induced apoptosis is closely linked to the subcellular distribution of Nrf2. These findings support the notion that ROS accumulation mediates AD-induced apoptosis in Burkitt's lymphoma cells.

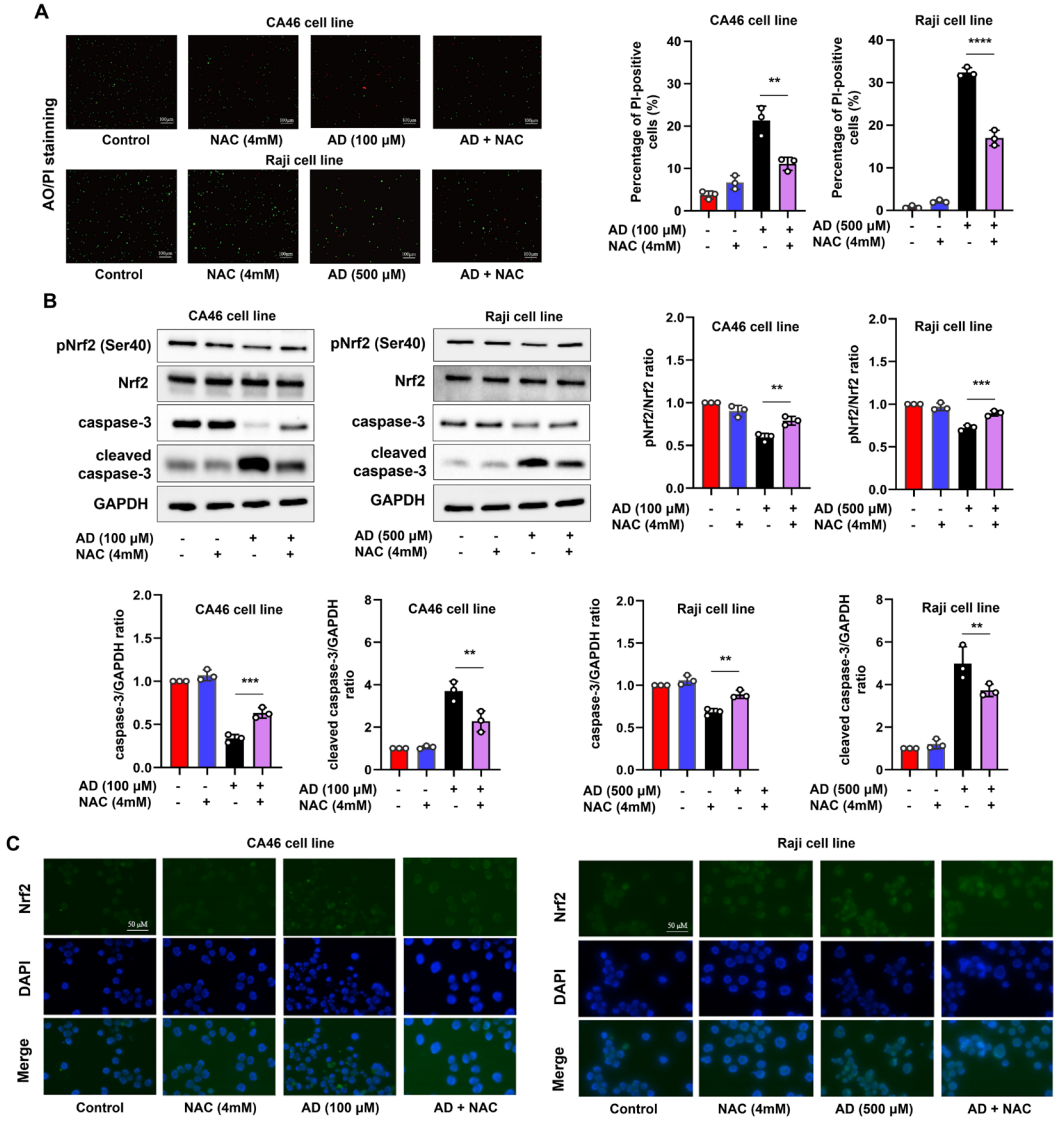


Fig. 6. NAC alleviated AD-induced cytotoxicity in Burkitt's lymphoma cells. (A) AO/PI staining was used to assess the ability of the ROS scavenger NAC to rescue cells from AD-induced death. (B) Representative Western blots and quantitative analyses of caspase-3 and cleaved caspase-3 and the phosphorylation level of Nrf2. (C) Immunofluorescence staining was used to analyze the subcellular localization of Nrf2. **P<0.01, ***P<0.001, ****P<0.0001 denote P values between "AD" group and "AD + NAC" group. Experiments were performed in triplicate (n = 3).

Discussion

Burkitt's lymphoma is characterized by MYC translocation, which drives an exceptionally rapid proliferative rate, often reflected by a Ki-67 index approaching 100% [24]. Given this aggressive clinical behavior, conventional chemotherapy frequently fails to achieve total tumor eradication, inevitably leading to the emergence of drug-resistant clones. To counteract this intrinsic aggressiveness, high-intensity, dose-dense regimens—such as R-CODOX-M/R-IVAC or DA-EPOCH-R are typically employed to rapidly reduce tumor burden. While the integration of the CD20-directed monoclonal antibody rituximab has improved clinical outcomes, reduced recurrence rates, and demonstrated a positive trend in progression-free and overall survival [25], a substantial subset of patients remains resistant to these approaches. The management of Burkitt's lymphoma is further complicated by specific

clinical challenges. Central nervous system (CNS) involvement occurs in 5% to 40% of cases [26]. However, the limited penetration of conventional agents across the blood-brain barrier renders CNS disease a frequent and major site of relapse. Furthermore, approximately 20% of patients experience either primary refractory disease or early recurrence, clinical settings in which standard regimens are often ineffective and prognosis remains dismal. Consequently, there is an urgent need for novel therapeutic agents. AD, a bioactive compound derived from *Andrographis paniculata*, has recently emerged as a promising candidate. Previous research has demonstrated that AD can induce ferroptosis in non-small cell lung cancer and other malignancies by modulating the SLC7A11/GPX4 and Nrf2/HO-1 signaling pathways, as well as by triggering mitochondrial dysfunction [18-21]. However, the efficacy and mechanism of AD in the context of Burkitt's lymphoma remain largely unexplored. This study seeks to investigate whether AD can effectively inhibit Burkitt's lymphoma cell growth and elucidate whether its mechanism of action involves the induction of ferroptosis.

Our findings diverge from previous literature regarding the role of AD in ferroptosis. Contrary to reports in lung and other solid tumors, we observed that AD failed to induce ferroptosis in Burkitt's lymphoma cells. This was evidenced by the lack of sensitivity to the ferroptosis inhibitor Ferrostatin-1 and the absence of significant alterations in markers of lipid peroxidation, such as MDA levels and intracellular Fe^{2+} content. Furthermore, AD treatment led to the upregulation of the ferroptosis-suppressive proteins GPX4, alongside the downregulation of the pro-ferroptotic enzyme ACSL4, collectively indicating that ferroptosis is not the primary mechanism of cell death in this context. Instead, our data suggest that impaired Nrf2-related antioxidant defense may be involved in AD-induced apoptosis. We observed that AD treatment decreased Nrf2 phosphorylation, which correlated with elevated ROS levels and increased cleaved caspase-3 expression. Nrf2 is a pivotal regulator of both redox homeostasis and anti-apoptotic signaling. Thus, its impaired phosphorylation likely compromises the cellular antioxidant capacity, thereby initiating the intrinsic apoptotic cascade. This pro-apoptotic shift was confirmed by an altered Bax/Bcl-2 ratio, a significant upregulation of Bax and downregulation of Bcl-2, indicative of a pro-apoptotic mitochondrial state. To further elucidate this mechanism, we utilized NAC, an antioxidant precursor that boosts glutathione synthesis and restores redox balance. Our results showed that NAC supplementation significantly mitigated AD-induced cell death, partially restored Nrf2 phosphorylation, and attenuated the upregulation of cleaved caspase-3. Collectively, these findings suggest that AD induces apoptosis in Burkitt's lymphoma by inhibiting the antioxidant response, rather than by triggering ferroptosis.

As a transcription factor, Nrf2 directly binds to a specific sequence in the promoter region of the Bcl-2 gene, which contains a critical antioxidant response element (ARE) [27]. Through an ARE-dependent mechanism, Nrf2 upregulates Bcl-2 expression, representing a key molecular pathway by which tumor cells evade chemotherapy-induced apoptosis and promote survival and drug resistance [28]. This finding provides a theoretical foundation for developing combination therapies targeting the Nrf2/Bcl-2 axis. Protein kinase C (PKC) family members phosphorylate Nrf2 at Ser40, a modification that reduces the affinity of Nrf2 for Keap1 and leads to partial disruption of the Keap1-CUL3 ubiquitin ligase complex [29]. This phosphorylation enhances Nrf2 stability and accumulation, facilitating its translocation to the nucleus and resulting in coordinated activation of downstream gene expression [30]. However, a limitation of the present study is that it does not elucidate how AD downregulates Nrf2 phosphorylation at Ser40, nor does it confirm whether AD inhibits the transcriptional activity of Nrf2. Notably, the functional impact of Ser40 phosphorylation appears to be context-dependent, varying with cell type, stimuli, and concurrent signaling pathways. In some contexts, Ser40 phosphorylation contributes to Nrf2 activation, while in others, it may play a compensatory or redundant regulatory role, suggesting that Ser40 may not be strictly necessary for Nrf2 function [31].

In summary, AD exerts its cytotoxic effects on Burkitt's lymphoma cells primarily through the intrinsic apoptotic pathway rather than ferroptosis. These effects are likely mediated

by impaired Nrf2-related antioxidant defense and the resulting oxidative stress response. As our understanding of AD´s antitumor mechanisms and the pharmacological basis of its cytotoxicity becomes increasingly elucidated, this compound emerges as a promising candidate drug to broaden the therapeutic range for Burkitt's lymphoma.

Acknowledgements

Authors' contributions

HYL and QGF: conception and design, data analysis and interpretation, and manuscript writing. BK and TTW: collection and assembly of data, data analysis and interpretation, manuscript writing and revising. TTL: data collection and supervision of the experiments. All the authors have read and approved the final manuscript.

Funding Sources

This work was supported by Science and Technology Innovation Team of Nanchang Medical College (Project number NYTD202403), the Science and Technology Program of Jiangxi Administration of Traditional Chinese Medicine (grant numbers 2023B1190 and 2024B0385), and the Jiangxi Educational Department Foundation of China (grant numbers GJJ218913).

Statement of Ethics

The Burkitt's lymphoma cell lines (CA46 and Raji) were commercially obtained and are established, immortalized cell lines. This study did not involve human subjects or animals, so ethical approval was not required.

Disclosure Statement

The authors have no competing financial interests to declare.

References

1 Teras LR, DeSantis CE, Cerhan JR, Morton LM, Jemal A, Flowers CR. 2016 US lymphoid malignancy statistics by World Health Organization subtypes. *CA Cancer J Clin*. 2016;66(6):443-459.
2 Roschewski M, Staudt LM, Wilson WH. Burkitt's Lymphoma. *N Engl J Med*. 2022;387(12):1111-1122.
3 Grande BM, Gerhard DS, Jiang A, Griner NB, Abramson JS, Alexander TB, et al. Genome-wide discovery of somatic coding and noncoding mutations in pediatric endemic and sporadic Burkitt's lymphoma. *Blood*. 2019;133(12):1313-1324.
4 Schmitz R, Young RM, Ceribelli M, Jhavar S, Xiao W, Zhang M, et al. Burkitt's lymphoma pathogenesis and therapeutic targets from structural and functional genomics. *Nature*. 2012;490(7418):116-120.
5 Zhang W, Yang J, Zhou C, Hu B, Jin L, Deng B, et al. Early response observed in pediatric patients with relapsed/refractory Burkitt's lymphoma treated with chimeric antigen receptor T cells. *Blood*. 2020;135(26):2425-2427.
6 Short NJ, Kantarjian HM, Ko H, Khoury JD, Ravandi F, Thomas DA, et al. Outcomes of adults with relapsed or refractory Burkitt and high-grade B-cell leukemia/lymphoma. *Am J Hematol*. 2017;92(6):E114-E117.
7 Liu J, Kang R, Tang D. Signaling pathways and defense mechanisms of ferroptosis. *FEBS J*. 2022 Nov;289(22):7038-7050.
8 Jiang X, Yu M, Wang WK, Zhu LY, Wang X, Jin HC,et al. The regulation and function of Nrf2 signaling in ferroptosis-activated cancer therapy. *Acta Pharmacol Sin*. 2024 Nov;45(11):2229-2240.
9 Wang N, Zeng GZ, Yin JL, Bian ZX. Artesunate activates the ATF4-CHOP-CHAC1 pathway and affects ferroptosis in Burkitt's Lymphoma. *Biochem Biophys Res Commun*. 2019 Nov 12;519(3):533-539.

10 Rink JS, Lin AY, McMahon KM, Calvert AE, Yang S, Taxter T, et al. Targeted reduction of cholesterol uptake in cholesterol-addicted lymphoma cells blocks turnover of oxidized lipids to cause ferroptosis. *J Biol Chem*. 2021 Jan-Jun;296:100100.
11 Yu T, Xu-Monette ZY, Yu L, Li Y, Young KH. Mechanisms of ferroptosis and targeted therapeutic approaches in lymphoma. *Cell Death Dis*. 2023 Nov 25;14(11):771.
12 Shan X, Li S, Liu J, Wang C, Wei Y, Shi J, et al. The Therapeutic Potential of Andrographolide and Its Derivatives in Inflammatory Diseases. *Pharmacol Res Perspect*. 2025;13(5):e70161.
13 Dafur GS, Harun A, Kub TNT, Bakar RA, Harun A. A Systematic Review on the Antimicrobial Activity of Andrographolide. *J Microbiol Biotechnol*. 2024;35: e2408028.
14 Latif R, Wang CY. Andrographolide as a potent and promising antiviral agent. *Chin J Nat Med*. 2020;18(10):760-769.
15 Lu J, Ma Y, Wu J, Huang H, Wang X, Chen Z, et al. A review for the neuroprotective effects of andrographolide in the central nervous system. *Biomed Pharmacother*. 2019;117:109078.
16 Geng J, Liu W, Gao J, Jiang C, Fan T, Sun Y, et al. Andrographolide alleviates Parkinsonism in MPTP-PD mice via targeting mitochondrial fission mediated by dynamin-related protein 1. *Br J Pharmacol*. 2019;176(23):4574-4591.
17 Liu MY, Li HJ, Yang C, Zang WD, Liu ZD, Zhang L, et al. Insight into the pharmacological effects of andrographolide in musculoskeletal disorders. *Biomed Pharmacother*. 2022;146:112583.
18 Li J, Huang S, Wang Q, Zhou D, Zhao B, Yao J. Andrographolide promoted ferroptosis to repress the development of non-small cell lung cancer through activation of the mitochondrial dysfunction. *Phytomedicine*. 2023;109:154601.
19 Ullah A, Xing H, Wang X, Zhou C, Rui Z, Iqbal H, et al. Andrographolide Promotes Ferroptosis in Pancreatic Cancer via Targeting and Activating HSP90/GPX4 Ubiquitination. *Biofactors*. 2025;51(6):e70063.
20 Li W, Fu H, Fang L, Chai H, Ding B, Qian S. Andrographolide induced ferroptosis in multiple myeloma cells by regulating the P38/Nrf2/HO-1 pathway. *Arch Biochem Biophys*. 2023;742:109622.
21 Doi H, Akiyama H, Matsui T, Shiogama K, Hirayama M, Nakagawa R, et al. Andrographolide drives dual apoptosis and ferroptosis via caspase-3 and FACL4 in T-ALL cell lines. *Int J Hematol*. 2025;122(6):843-855.
22 Zeng J, Zheng Y, Dong S, Ding T, Zhang S, Li K, et al. Andrographolide inhibits Burkitt's lymphoma by binding JUN and CASP3 proteins. *Cancer Chemother Pharmacol*. 2024;93(4):381-391.
23 Yang S, Evens AM, Prachand S, Singh AT, Bhalla S, David K, et al. Mitochondrial-mediated apoptosis in lymphoma cells by the diterpenoid lactone andrographolide, the active component of Andrographis paniculata. *Clin Cancer Res*. 2010; 16 (19): 4755-4768.
24 Tsutsumi Y, Yanagita S, Ohshima K, Tachibana M. Adult Nodal Burkitt Lymphoma Forming Nodular Architectures. *Cureus*. 2021;13(10):e19130.
25 Barnes JA, Lacasce AS, Feng Y, Toomey CE, Neuberg D, Michaelson JS, et al. Evaluation of the addition of rituximab to CODOX-M/IVAC for Burkitt's lymphoma: a retrospective analysis. *Ann Oncol*. 2011;22(8):1859-1864.
26 Zayac AS, Evens AM, Danilov A, Smith SD, Jagadeesh D, Leslie LA, et al. Outcomes of Burkitt lymphoma with central nervous system involvement: evidence from a large multicenter cohort study. *Haematologica*. 2021;106(7): 1932-1942.
27 Niture SK, Jaiswal AK. Nrf2 protein up-regulates antiapoptotic protein Bcl-2 and prevents cellular apoptosis. *J Biol Chem*. 2012;287(13):9873-9886.
28 Jia Y, Chen J, Zhu H, Jia ZH, Cui MH. Aberrantly elevated redox sensing factor Nrf2 promotes cancer stem cell survival via enhanced transcriptional regulation of ABCG2 and Bcl-2/Bmi-1 genes. *Oncol Rep*. 2015;34(5):2296-2304.
29 Niture SK, Khatri R, Jaiswal AK. Regulation of Nrf2-an update. *Free Radic Biol Med*. 2014;66:36-44.
30 Bloom DA, Jaiswal AK. Phosphorylation of Nrf2 at Ser40 by protein kinase C in response to antioxidants leads to the release of Nrf2 from INrf2, but is not required for Nrf2 stabilization/accumulation in the nucleus and transcriptional activation of antioxidant response element-mediated NAD(P)H:quinone oxidoreductase-1 gene expression. *J Biol Chem*. 2003;278(45):44675-44682.
31 Kim DE, Byeon HE, Kim DH, Kim SG, Yim H. Plk2-mediated phosphorylation and translocalization of Nrf2 activates anti-inflammation through p53/Plk2/p21^{cip1} signaling in acute kidney injury. *Cell Biol Toxicol*. 2023;39(4):1509-1529.